Int. J. Electrochem. Sci., 15 **(2020)** 12068 – 12079, doi: 10.20964/2020.12.24

International Journal of
ELECTROCHEMICAL
SCIENCE
www.electrochemsci.org

Degradation of Malachite Green by Visible Light-Assisted Electrocatalytic Treatment Using N-V co-doped TiO_2 as Photocatalyst

Fuchen Ban[*], *Qiu Jin, Yanxin Wang*

School of Municipal and Environmental Engineering, Shenyang Jianzhu University, Shenyang 110168, China
[*]E-mail: optimms0809@163.com

Received: 26 July 2020 / *Accepted:* 14 September 2020 / *Published:* 10 October 2020

A γ-Al_2O_3-supported N-V co-doped TiO_2 (N-V/TiO_2/γ-Al_2O_3) photocatalyst was prepared as a particle electrode for a visible light-assisted multiphase electrocatalytic treatment. In this experiment, the Na_2SO_4 concentration, aeration, voltage and pH are used as variables, and COD removal is the response for multivariate optimization. The optimal condition for maximizing the COD removal of malachite green was obtained as Na_2SO_4 concentration of 0.12 moL/L, Voltage of 10.35V, Aeration of 51.9L/h and pH of 4. The optimal predicted and experimental COD removal were 86.94% and 86.17%. To study the intermediates and final products of malachite green degradation and further study the photoelectrochemical degradation pathway of malachite green, the solutions were sampled and pretreated for GC-MS analysis. A possible photoelectrochemical degradation pathway of MG were speculated. The visible light-assisted multiphase electrocatalytic method had a remarkable effect on the degradation of the simulated malachite green wastewater, and the operation was simple. By further optimizing the reaction conditions, it could be applied to the practice of malachite green removal in wastewater treatment engineering.

Keywords: electrocatalysis; visible light; photoelectrocatalysis; malachite green; intermediate product

1. INTRODUCTION

Malachite green is a triphenylmethane dye that is widely used in silk, cotton, leather, wood and paper industries as a colorant. Malachite green is widely used in many countries due to its low cost, high efficiency and lack of suitable substitutes. However, studies have found that when malachite green exists in the water, it will interfere with the transmission of sunlight, reduce the photosynthesis of plants, and thus affect the living environment of aquatic organisms [1-2]. Moreover, malachite green can also harm the human body by affecting the human immune system and reproductive system [3]. In

2002, malachite green was listed as a major chemical carcinogen by the US Food and Drug Administration. Therefore, it is very important to explore effective methods to remove this substance from water bodies. Electrochemical catalysis technology is easy to operate and provides a clean process [4]. Further, this process as it is carried out today combines both photocatalytic oxidation and electrochemical oxidation. Hence, this technology reduces the problems of large energy consumption, high processing cost, and low current efficiency that are typically associated with traditional electrochemical catalysis methods. However, most photoelectrocatalytic research focuses on ultraviolet light, and artificial ultraviolet light sources have the disadvantages of large power consumption, expensive equipment, and poor stability. The application of new nanocomposites in the field of sewage treatment has been extensive [5-8]. The optimization of variables through the response surface method (RSM) can better show the interaction between variables and help optimize the degradation process through fewer experiments.

In this study, an N-V/TiO_2/γ-Al_2O_3 particle electrode was prepared with malachite green as the target pollutant. The visible light catalysis of nano-TiO_2 was improved by N-V co-doping. This experiment investigates the influence of various factors on the visible light-assisted multiphase electrocatalytic degradation of MG and its operating range by changing one variable at a time. The response surface method with BBD experimental design was used to optimize the operating parameters of photoelectrochemical degradation. Furthermore, the degradation pathway of malachite green was analysed by GC-MS.

2. MATERIALS AND METHODS

Slowly add 40mL of absolute ethanol to 13.6mL of tetrabutyl titanate, and continue to stir during the addition to make it fully react. After stirring for 30 minutes, solution A was obtained. 10 mL of absolute ethanol, 2 mL of glacial acetic acid and 2 mL of deionized water were mixed and continuously stirred in a magnetic stirrer to obtain solution B in 30 minutes. Add 5g of γ-Al_2O_3 pretreated with dilute acid to solution A, use a magnetic stirrer to continue mixing and stirring thoroughly, and slowly add solution B to solution A after γ-Al_2O_3 is evenly mixed. Continue to add urea and NH_4VO_3 as N source and V source in the mixture. The doping ratio of N was controlled to 20%, and the doping ratio of V was 0.7%, 0.8%, 0.9%, 1.0%, and 1.1%, respectively. Five samples were marked as T1, T2, T3, T4 and T5. After all the abovementioned additions, the solution was stirred vigorously for 30 min and N-V/TiO_2/γ-Al_2O_3 sol was obtained. After standing at room temperature, it was air-dried to a dry gel. Next, the sample was calcined at 400°C for 3 hours in a muffle furnace to obtain a series of differently doped samples of N-V/TiO_2/γ-Al_2O_3 powder.

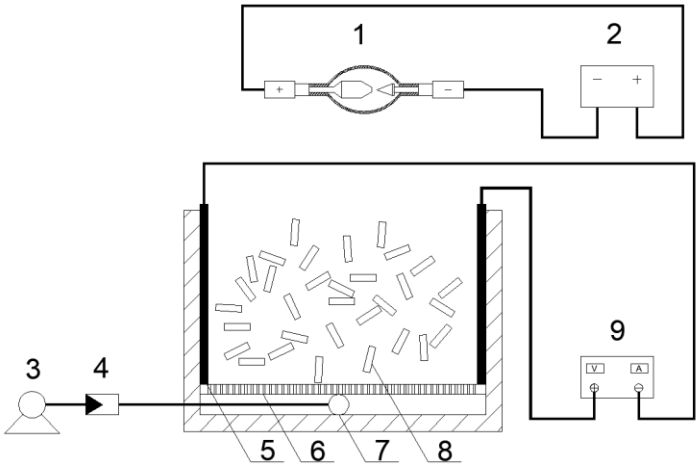

1-Short arc Xenon lamp, 2-Xenon lamp power supply, 3-Air compressor, 4-Rotor flowmeter, 5-IrO_2/Ti anode plate and titanium cathode plate, 6-Aeration plate, 7-Aeration plate inlet, 8-N-V/TiO_2/γ-Al_2O_3 particle electrode, and 9-regulated power supply

Figure 1. Schematic of the experimental device.

In this experiment, a malachite green solution with a concentration of 150 mg/L was used to produce simulated wastewater. A 350 W xenon lamp was used as the visible light source, and a 2 mol/L sodium nitrite aqueous solution was prepared in a reactor jacket to filter out most of the ultraviolet light. The effective processing volume of the electrolytic reactor was 14 cm × 12 cm × 10 cm. The effective oxidation area of the plate was 10 cm × 10 cm. As an electrocatalytic anode, titanium-based DSA material has high oxygen evolution overpotential, high electrochemical stability and corrosion resistance. Therefore, the selected anode was a IrO_2/Ti plate because its oxide coating has a low chlorine evolution overpotential and a high oxygen evolution overpotential; additionally, the above anode demonstrates catalytic activity and is resistant to electrical contact friction. The cathode was a titanium plate, and a particle electrode was placed in the reactor. The simulated malachite green wastewater was put into the reactor, and then a certain amount of Na_2SO_4 electrolyte and acid-base reagent were added. The air compressor was turned on to aerate the reactor and control the aeration volume through a rotor flow meter. Then, the cooling fan and xenon lamp were turned on, and the DC-regulated power supply was adjusted to output a certain voltage. The malachite green wastewater was sampled at intervals of 20 min for a total of 120 min. The COD was determined by rapid closed catalytic digestion, and the degradation rate of malachite green was calculated by 4-aminoantipyrine direct spectrophotometry.

3. RESULTS AND DISCUSSION

3.1. Catalyst characterization

Figure 2 shows that the absorption intensity of the sample prepared at a 400 °C calcination

temperature in a light absorption range of 380-670 nm increased significantly. This shows that the N-V co-doping increased the photocatalytic activity of the sample. It is convenient to generate more photogenerated electron holes at higher wavelengths, and the best sample is T_2. As the doping amount of V^{5+} increases further, the absorbance of the sample decreases, which increases the probability of photogenerated electron-hole recombination and decreases the photocatalytic performance of the sample.

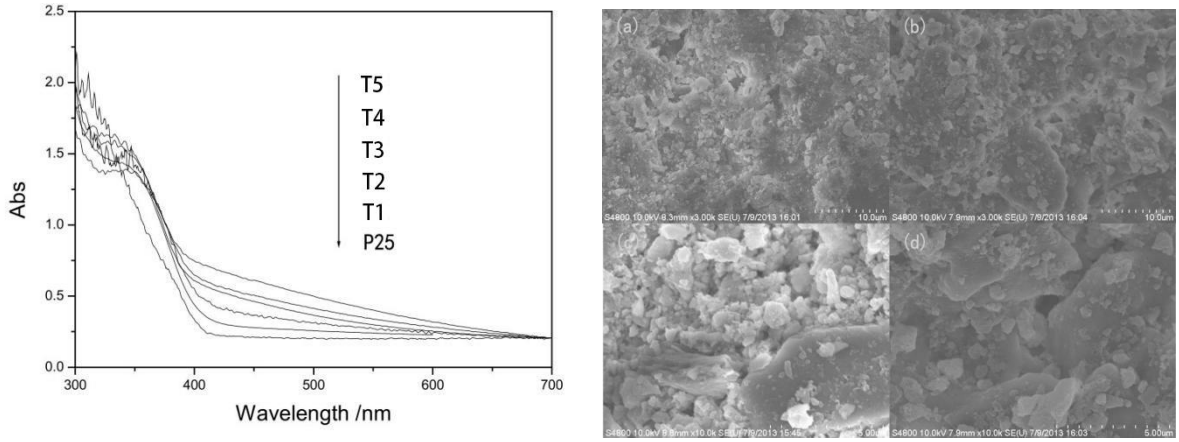

(a) (b)

Figure 2. UV-visible light absorption curves of N-V/TiO_2/γ-Al_2O_3 (a) and SEM images of various catalysts (b) (a and c are electron micrographs of γ-Al_2O_3 at 3000x and 10000x magnifications, respectively; b and d are electron micrographs of N-V/TiO_2/γ-Al_2O_3 at 3000x and 10000x magnifications, respectively).

Figure 2 (b) shows the microstructure of the catalyst under scanning electron microscopy. As can be clearly seen from the comparison, the γ-Al_2O_3 support has an uneven surface before the catalytically active component is loaded; additionally, the support has a distinct void structure. After loading the active components, the surface of the catalyst N-V/TiO_2/γ-Al_2O_3 becomes smooth, obvious crystal forms can be observed, and the crystal structure is stable. The specific surface area and surface roughness of the sample are both large, which meets the requirements of catalyst porosity.

3.2. Effect of pH, voltage and aeration

The effect of pH on the removal rate of malachite green COD is shown in Figure 3a. Under acidic conditions, a reduction reaction occurs on the surface of the cathode to produce strongly oxidizing ·OH and H_2O_2. At this time, the oxygen is also more oxidative, which is beneficial to the degradation of organic matter in the solution; thus, the malachite green removal rate is high. In the catalysis process, the pollutants are first adsorbed to the surface of the catalyst N-V/TiO_2/γ-Al_2O_3, and then the catalytic active sites under light conditions are used to degrade the pollutants. pH has an

activating effect on active sites, just as the oxidation performance of potassium permanganate is stronger under acidic conditions. In addition, the lower the pH, the stronger the ability of the catalyst to adsorb pollutants. Increasing pH causes the existing form of malachite green to change, and severe side reactions on the plate will compete with the organic matter, which is not conducive to its degradation and affects the removal of malachite green. Therefore, a significant decline was observed in MG being removed in this case. From the above analysis, it can be seen that in the electrochemical reaction, acidic conditions are favourable for the removal of organic matter, and the initial pH requirements are very strict.

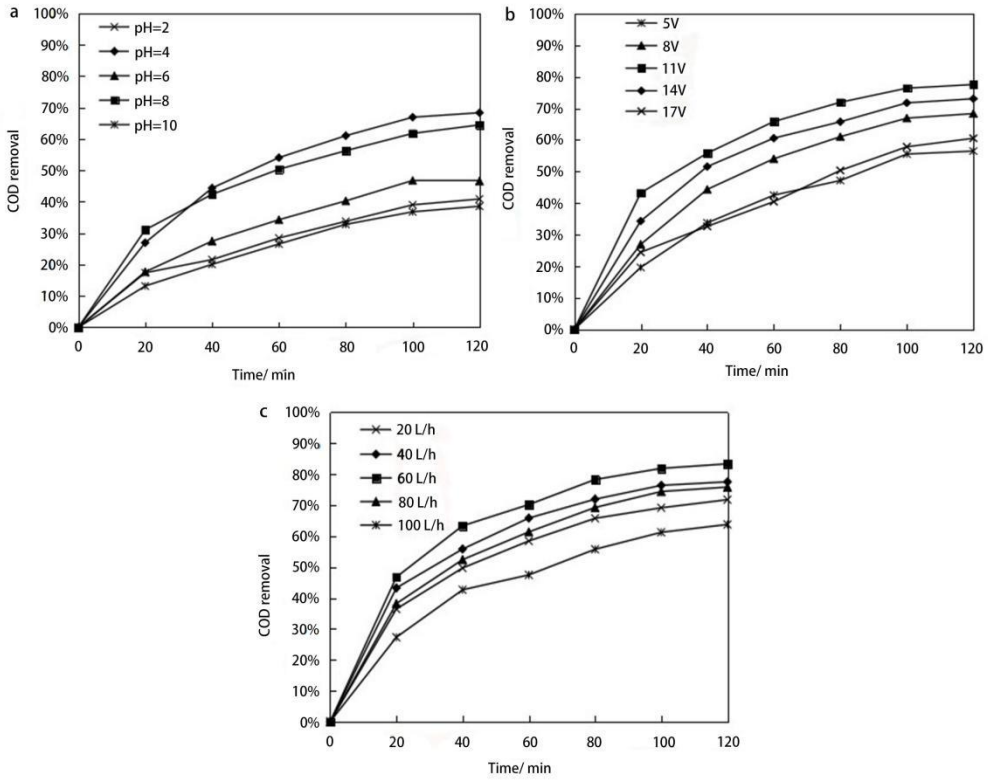

Figure 3. COD removal efficiency of MG (150mg/L) at (a) varying initial pH (initial concentration—150 mg/L, N-V/TiO_2/γ-Al_2O_3 particle electrode — 35g/L, voltage—8V, aeration—40L/h); (b) varying voltage (initial concentration—150 mg/L, N-V/TiO_2/γ-Al_2O_3 particle electrode— 35g/L, initial pH—4, aeration—40L/h); (c) varying aeration (initial concentration—150 mg/L, N-V/TiO_2/γ-Al_2O_3 particle electrode — 35g/L, initial pH—4, voltage—11V).

The effect of voltage on the removal rate of malachite green is shown in Figure 3b. With the increase of voltage, the number of N-V/TiO_2/γ-Al_2O_3 particle electrodes being polarized increases and the contact area increases, and under the action of light irradiation, the recombination of electron-hole pairs is inhibited, which is beneficial to the generation of strong oxidizing substances. However, a high voltage leads to increased energy consumption and reduced selectivity for malachite green degradation [9]. Fierro [10] and Simond [11] studied the mechanism of catalytic degradation of organics by IrO_2-coated electrodes, as shown below:

$(IrO_2)_s + H_2O \rightleftarrows (IrO_2)s[\bullet OH] + H^+ + e^-$ (1)

$(IrO_2)_s [\bullet OH] \rightarrow (IrO_3)_s + H^+ + e^-$ (2)

$(IrO_3)_s \rightarrow (IrO_2)_s + 1/2\ O_2$ (3)

$(IrO_3)_s + R_{ad} \rightarrow (IrO_2)_s + (RO)_{ad}$ (4)

In this degradation model, water molecules are first oxidized by IrO_2 on the anode surface to form hydroxyl species that are adsorbed on the anode surface. The adsorbed hydroxyl species will form chemisorbed oxygen and simultaneously oxidize organic matter. The catalyst is then reduced to IrO_2, but a part of this IrO_3 decomposes to generate oxygen which is a side reaction.. The increase in voltage intensifies the occurrence of side reactions in the three-dimensional electrode system composed of the cathode and anode plates and the N-V/TiO_2/γ-Al_2O_3 particle electrodes, and at the same time increases the power consumption.

The influence of aeration on the removal rate of malachite green is shown in Figure 3c. The malachite green removal rate increased from 63.76% to 83.35% as aeration increased from 20 L/h to 100 L/h. According to Xiong [12] and Siracusano [13], aeration keeps the particle electrode in a suspended state, which can reduce the generation of a short-circuit current. The number of repolarizations of the N-V/TiO_2/γ-Al_2O_3 particle electrodes increases, and the mass transfer efficiency is also improved. Aeration can provide oxygen to rapidly generate H_2O_2 and ·OH. Electrons generated by electric field excitation can also be captured on the catalyst surface to inhibit the recombination of electrons and holes, thereby generating hydroxyl radicals, as shown below:

$O_2+2H^++2e \rightarrow H_2O_2$ （5）

$H_2O_2+H^+ \rightarrow \cdot OH+H_2O$ （6）

$2H^++2e^-_{aq} \rightarrow H_2$ （7）

When the aeration rate continues to increase to 100 L/h, the malachite green removal rate decreases significantly. Excessive aeration makes it impossible for organic matter to stay on the surface of the N-V/TiO_2/γ-Al_2O_3 particle electrodes, leaving it before reacting with the active material that is generated on the electrode surface; thus, excessive aeration is not conducive to the oxidative degradation of organic matter on the electrode surface. Furthermore, excessive aeration increases the probability of contact between the N-V/TiO_2/γ-Al_2O_3 particle electrodes, resulting in an increase in short-circuit current and a reduction in the removal rate.

3.3. Multivariate optimization

Table 1. Experimental design.

Sl. no	A-Na_2SO_4 concentration, （moL/L）	B-Aeration （L/h）	C-Voltage (V)	D-pH	COD removal (%)
1	0.15	50	11	4	84
2	0.1	20	11	4	75
3	0.1	20	14	6	69
4	0.15	20	11	6	78
5	0.1	20	8	6	79

6	0.15	50	11	8	77
7	0.1	50	11	6	85
8	0.15	80	11	6	78
9	0.05	50	8	6	67
10	0.1	80	11	8	82
11	0.05	50	11	4	66
12	0.15	50	14	6	70
13	0.1	50	11	6	84
14	0.1	20	11	8	72
15	0.05	50	14	6	68
16	0.15	50	8	6	82
17	0.1	50	11	6	85
18	0.05	50	11	8	70
19	0.1	50	8	4	76
20	0.1	50	14	8	75
21	0.05	20	11	6	67
22	0.1	80	8	6	74
23	0.1	80	14	6	81
24	0.1	50	11	6	85
25	0.1	80	11	4	79
26	0.1	50	8	8	81
27	0.1	50	14	4	80
28	0.15	50	11	4	84
29	0.1	20	11	4	75

Experimental design was established for four variables (Na_2SO_4 concentration, voltage, aeration volume and pH) and one response (COD removal). The initial concentration of MG was 150 mg/L and N-V/TiO_2/γ-Al_2O_3 particle concentration was 35g/L. In this experiment, Design Expert 8.0.6 software was used to sort and analyze the experimental results, and the data in Table 1 was fitted with a quadratic polynomial, and the quadratic multiple regression model was obtained as:

COD removal= + 90.40- 1.42A- 0.33B+ 1.83C+ 5.25D- 2.25AB+ 4.25AC- 3.25AD+ 1.5BC- 2.75BD- 0.25CD- 4.78 A^2-2.91B^2- 4.91C^2- 8.28D^2

Table 2. ANOVA for the response surface quadratic model

Source	Sum of Squares	df	Mean Square	F-Value	P-Value	Significance
Model	1142.03	14	81.57	23.17	< 0.0001	significant
A-Na_2SO_4 concentration,	24.08	1	24.08	6.84	0.0203	*
B-Aeration volume	1.33	1	1.33	0.38	0.5481	
C-Voltage	40.33	1	40.33	11.46	0.0044	**
D-pH	330.75	1	330.75	93.96	< 0.0001	**
AB	9	1	9	2.56	0.1321	
AC	20.25	1	20.25	5.75	0.031	*

AD	42.25	1	42.25	12	0.0038	**
BC	30.25	1	30.25	8.59	0.0109	*
BD	0.25	1	0.25	0.071	0.7937	
CD	72.25	1	72.25	20.52	0.0005	**
A^2	148.41	1	148.41	42.16	< 0.0001	**
B^2	54.87	1	54.87	15.59	0.0015	**
C^2	156.27	1	156.27	44.39	< 0.0001	**
D^2	445.06	1	445.06	126.43	< 0.0001	**
Residual	49.28	14	3.52			
Lack of Fit	46.08	10	4.61	5.76	0.0531	not significant
Pure Error	3.2	4	0.8			
Cor Total	1191.31	28	R^2	0.9586	R^2 adj	0.9173

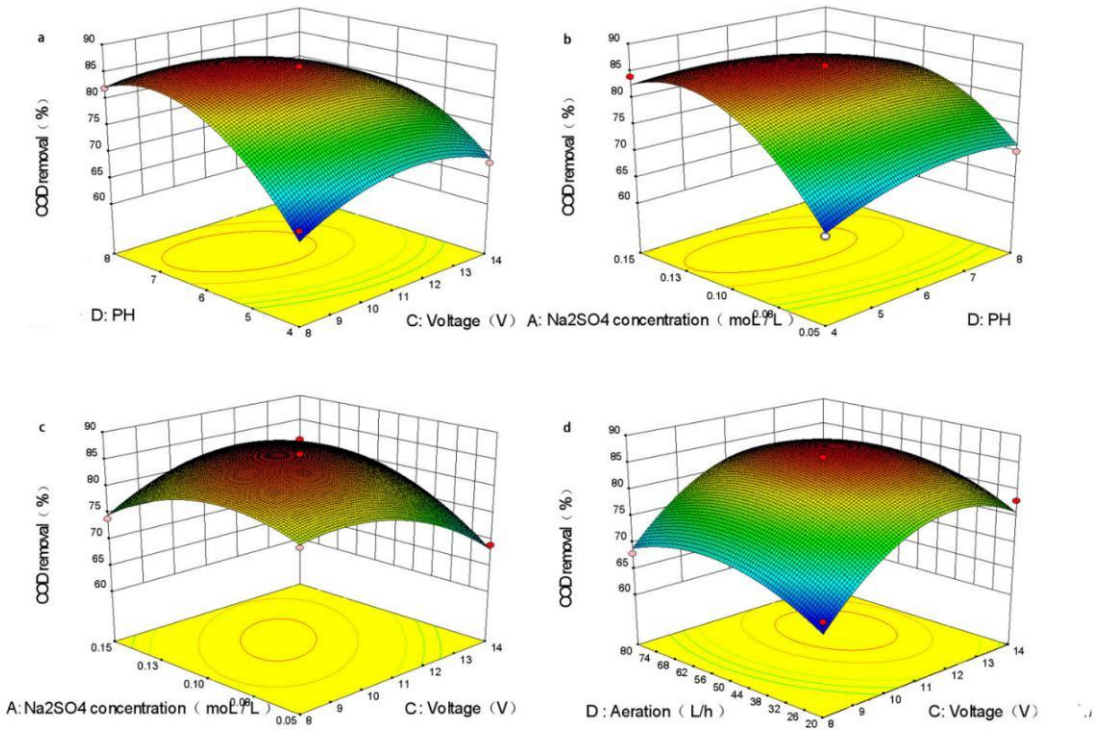

Figure 4. 3D surface plots for (a) pH and voltage versus COD removal, (b) Na_2SO_4 concentration and pH versus COD removal, (c) Na_2SO_4 concentration and voltage versus COD removal, and (d) aeration and voltage versus COD removal.

From the results of the analysis of variance, it can be seen that the P value of the regression model is less than 0.01, and the lack of fit term P=0.0531>0.05, indicating that the residuals are all caused by random errors. The model determination coefficient R^2=0.9586, R^2_{Adj}=0.9173, indicating that the model can explain 91.73% of the change in response value, and the model fits well with the experiment. It can be seen from the analysis of variance table that voltage, Na_2SO_4 concentration and aeration volume have significant effects on the COD removal. The greater the mean square value, the

greater the impact. Therefore, the order of the four factors affecting the COD removal is D>C>A>B, that is, pH>voltage>Na_2SO_4 concentration>aeration volume. The interaction between AD and CD was extremely significant ($P<0.01$), the interaction between AC and BC was significant ($P<0.05$), and the interaction between AD and BD was not significant ($P>0.05$).

Interactive effect plots of the variables on COD removal are provided in Figure 4a-d. In the COD removal model, the interaction between Na_2SO_4 concentration and initial pH was observed to be significant. It can be seen from Figure 4a that the response surface is steep, so the interaction of pH and Voltage has a greater impact on the COD removal. The curved axis of pH is steeper than that of Voltage, indicating that pH has a greater impact on COD removal. With the increase of pH and Voltage, the COD removal first increases and then decreases, indicating that an appropriate increase in pH and Voltage is beneficial to increase the removal rate, but the continuous increase of the two factors is unfavorable for the COD removal. As mentioned before, the increase in pH value will cause serious side reactions on the plate to compete with organic matter, which is not conducive to its degradation and affects the COD removal. There is also a similar interaction between voltage and Na_2SO_4 concentration, which is consistent with the results of analysis of variance.

Within the tested parameters, the optimal operating conditions are optimized to achieve the maximum COD removal. The optimum conditions were obtained at Na_2SO_4 concentration of 0.12 moL/L, Voltage of 10.35V, Aeration of 51.9L/h and pH of 4. The predicted COD removal efficiency at these conditions was 86.94%. The reaction conditions are adjusted at Na_2SO_4 concentration of 0.12 moL/L, Voltage of 10V, Aeration of 52L/h and pH of 4. The COD removal obtained under this condition is 86.17%, which is close to the theoretical prediction value.

3.4. Discussion on the action mechanism of visible light-assisted electrocatalysis

N-V/TiO_2 is the active ingredient in N-V/TiO_2/γ-Al_2O_3 particle electrode. In an N-doped nano-TiO_2 semiconductor, N^{3-} replaces part of the O^{2-} in the TiO_2 lattice, which generates oxygen vacancies. Oxygen vacancies generate impurity levels in the forbidden band of nano-TiO_2, making the forbidden band width smaller. N^{3-} can also enter the TiO_2 lattice gap and is highly dispersed in the crystal lattice, thereby shortening the band gap width and broadening the optical absorption range [14-15]. The forbidden band width of the V_2O_5 semiconductor is 2.05 eV [16]. When V^{5+} ions are doped into the TiO_2 lattice, the photogenerated electrons on the TiO_2 conduction band can jump to the V_2O_5 conduction band so that photogenerated electron-hole transfer occurs [17].

The radius of N^{3-} (0.13 nm) is slightly smaller than that of O^{2-} (0.14 nm). N^{3-} can enter the TiO_2 lattice, replacing O^{2-} in the crystal lattice to form Ti-N-O bonds, or enter the lattice gap of TiO_2 [18]. The radius of V^{5+} is 59 pm, which is close to the radius of Ti^{4+} (68 pm). V^{5+} can replace Ti^{4+} at its lattice position to reduce the grain size and increase the unit cell volume [19]. As the N^{3-} doping amount increases, the intermediate impurity energy level will also increase, and new O 2p orbitals will be formed. The potential of the new O 2p orbit is higher than that of the original O 2p orbit, and the electrons are more likely to transition to the conduction band. Therefore, the valence band of TiO_2 is increased while the band gap value is small, which broadens the absorption spectrum.

Photocatalyst TiO_2-doped ions generally include transition metal ions, rare earth metal ions, precious metal ions, inorganic ions, and other ions [20-24]. Appropriate ion doping can generally enhance the absorption intensity of TiO_2 in the visible range, but the photocatalytic activity of doped TiO_2 is related to many factors, such as the type of doped ions, concentration, preparation method and post-treatment. In^{3+}/TiO_2, B/TiO_2, Nd^{3+}-N/TiO_2 and V-N/TiO_2 photocatalysts can be prepared by a sol-gel method. A tangent method is used to calculate the absorption threshold (λonset) and band gap (Eg) of the sample, as shown in Table 1. N-V co-doped nano-TiO_2 has a maximum redshift of 71 nm, which improves the photocatalytic efficiency of TiO_2; the above redshift is followed by that of In^{3+}-doped nano-TiO_2, with a redshift of 68 nm. This shows that metal and non-metal co-doped TiO_2 has better application prospects in wastewater treatment. Non-metal-doped TiO_2 is supported on activated carbon, γ-Al_2O_3 and other carriers, which can be better applied to photoelectric co-processing of organic wastewater.

Table 3. The absorption threshold (λonset) and band gap (Eg) of In^{3+}/TiO_2, B/TiO_2, Nd^{3+}-N/TiO_2 and V-N/TiO_2 photocatalysts [24]

	In^{3+}/TiO_2	B/TiO_2	Nd^{3+}-N/TiO_2	V-N/TiO_2
λg (nm)	494.45	448.42	463.29	497.25
Eg (eV)	2.51	2.77	2.68	2.49

3.5. Pathway of degradation

In this experiment, GC-MS was used to analyse the degradation mechanism of MG in the photoelectrochemical degradation process. In the process of photoelectrochemical reaction, MG molecules and intermediates will be attacked by active free radicals, which may involve many complex reactions such as N-demethylation reaction, benzene removal reaction and ring opening reaction [25-28].

First, in the aqueous solution of malachite green, the main structure is separated from Cl^- and becomes the positively charged MG* [29]. Due to •OH's attack on the central carbon atom and the process of demethylation, MG* is converted to (4-aminophenyl) (4-(methylamino) phenyl) (phenyl) methanol. The central carbon of malachite green undergoes a hydroxylation reaction, and then the central carbon rapidly breaks the carbon-carbon bond to produce 4,4-bis(dimethylamino) benzophenone and phenol. 4,4-bis(dimethylamino) benzophenone will continue to be oxidized into organic compounds such as N,N-dimethylaniline, 4-dimethylaminobenzoic acid, p-Nitrobenzoic acid and 4-Hydroxybenzoic acid [30]. Phenol is oxidized to organic compounds such as Hydroquinone and p-Benzosemiquinoneand, and then further mineralized into small molecular organic compounds [31]. According to the results above, a possible photoelectrochemical degradation pathway of MG were speculated and presented in Figure 5.

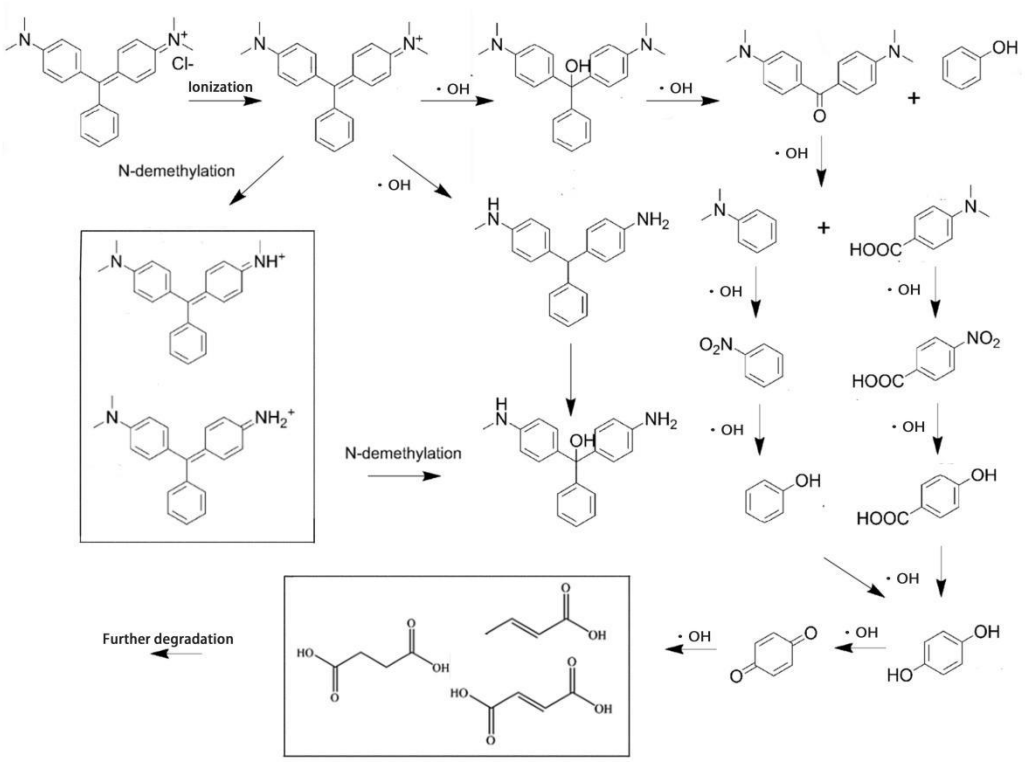

Figure 5. Proposed pathway of photoelectrochemical degradation of MG

4. CONCLUSIONS

A simulated malachite green wastewater was treated by visible light-assisted multiphase electrocatalysis. An N-V/TiO_2/γ-Al_2O_3 catalyst was used as a particle electrode. The particle electrode exhibits good photoelectrocatalytic performance in the visible light-assisted multiphase electrocatalytic system. The optimum conditions were obtained at Na_2SO_4 concentration of 0.12 moL/L, Voltage of 10.35V, Aeration of 51.9L/h and pH of 4. The predicted COD removal efficiency at these conditions was 86.94%. The reaction conditions are adjusted at Na_2SO_4 concentration of 0.12 moL/L, Voltage of 10V, Aeration of 52L/h and pH of 4. The COD removal obtained under this condition is 86.17%. A possible pathway of MG degradation was proposed with the identified intermediates by GC-MS. MG molecules undergo many complex reactions, such as N-demethylation reaction, benzene removal reaction, and ring opening reaction to generate a series of intermediate products. By further optimizing the reaction conditions, the visible light-assisted multiphase electrocatalytic method can be applied to the practice of malachite green removal in wastewater treatment engineering.

ACKNOWLEDGMENTS
This work was financially supported by Liaoning Natural Science Fund Project under Grant number 2014020073.

References

1. X. Xiong, X. Zhang and Y. Xu, *The Journal of Physical Chemistry C*, 120 (2016) 25689.
2. C.D. Luca, F. Ivorra, P. Massa and R. Fenoglio, *Chemical Engineering Journal*, 268 (2015) 280.
3. X. Sun, Q. Zhang, H. Liang, L. Ying and V.K. Sharma, *Journal of hazardous materials*, 319 (2015) 130.
4. M.B. Gholivand and A. Azadbakht, *Materials Science & Engineering*, 32 (2019) 1955.
5. F.Z. Haque, R. Nandanwar, P. Singh. *Optik - International Journal for Light and Electron Optics*, 128 (2017) 191.
6. H. You, Z. Wu, Y. Jia, X. Xu, Y. Xia and Z. Han, *Chemosphere*, 183 (2017) 528.
7. Y.J. Deng, Y. Liu and X.H. Yang, *European Journal of Inorganic Chemistry*, 22 (2015) 3708.
8. F. Liang and Y. Zhu, *Applied Catalysis B: Environmental*, 180 (2016) 324.
9. M. Li, Q. Xue, Z. Zhang, C. Feng, N. Chen, X. Lei, Z. Shen and N. Sugiura, *Electrochimica Acta*, 55 (2010) 6979-6982.
10. S. Fierro and C. Comninellis, *Electrochimica Acta*, 55 (2010) 7067.
11. O. Simond and C. Comninellis, *Electrochimica Acta*, 42 (1997) 2013.
12. Y. Xiong, C. He, H.T.Karlsson, Chemosphere, 50 (2003) 131.
13. S. Siracusano, V. Baglio, A. Stassi, R. Ornelas, V. Antonucci and A.S. Aricò, *International Journal of Hydrogen Energy*, 36 (2011) 7822.
14. Z.L. Cheng and S. Han, *Water Science and Technology*, 73 (2016) 486.
15. L. Suhadolnik, A. Pohar and B. Likozar, *Chemical Engineering Journal*, S1385894716308348 (2016) .
16. L.D. Than, N.S. Luong and V.D. Ngo, *Journal of Electronic Materials*, 46 (2017) 1.
17. X.J. Li, D.J. Si and J. Fang, *J. Phys. Chem.*, 27 (2006) 539.
18. N.N. Ilkhechi, N. Ghobadi and M.R. Akbarpour. *Journal of Materials Science Materials in Electronics*, 28 (2017) 6426.
19. C.X. Li, Z.Y. Zhao, S.L. Hamukwaya, *Journal of Materials Research*, 32 (2016) 737.
20. L. Gao, S. Zheng, Q.H. Zhang, Nano titanium oxide photocatalytic material and application, Beijing: Chemical Industry Press, 2002.
21. Y.H. Ao, J.J. Xu, *Mierop Mesop Mater*, 122 (2009) 1.
22. F.Y. Wei, L.S. Ni, Journal of Catalysis, 28 (2007) 905.
23. X.F. Zhao, Z.H.Zhang, X.F. Meng, *Molecular catalysis*, 17 (2003) 292.
24. G.L. Liu, C.S Han, M. Pelaez, *Molecular Catalysis A: Chemical*, 37 (2013) 58.
25. T. Ohno, M. Akiyoshi, T. Umebayashi, Catal A, 265(2004) 115.
26. X.Y. Li, Y.H. Cui, Y.J. Feng, *Water Research*, *39* (2014) 1972.
27. C.D. Luca, F. Ivorra, P.Massa and R. Fenoglio, *Chemical Engineering Journal*, 268 (2015) 280.
28. I. Ali, S.R. Kim, S.P. Kim and J.O. Kim, *Catalysis Today*, S0920586116301985 (2016).
29. A.P. Sarmento, A.C. Borges, A.T. De Matos and L.L. Romualdo, *Environmental Science and Pollution Research*, *23* (2016) 18429.
30. A.Amin, N.Davood, *Water Research*, 144 (2018) 462.
31. H. Wu. *Journal of Hazardous Materials*, 321 (2017) 408.